

## Article

# Synthesis and Characterization of Eco-Friendly Nanocomposites Using Galactomannan and Organomodified Montmorillonite

Razika Saihi <sup>1,2</sup>, Lahcene Souli <sup>3</sup>, Salem Fouad Chabira <sup>2</sup>, Yazid Derouiche <sup>4,\*</sup>  and Ulrich Maschke <sup>5,\*</sup> 

<sup>1</sup> Technological Hall, University Ziane Achour of Djelfa, P.O. Box 3117, Djelfa 17000, Algeria; r.saihi@lagh-univ.dz

<sup>2</sup> Laboratory of Mécanics, Faculty of Technology, University Amar Tlidji, Laghouat 03000, Algeria; s.chabira@lagh-univ.dz

<sup>3</sup> Laboratory of Organic Chemistry and Naturel Substance (LOCNa), Faculty of Exact Sciences and Computer Science, University of Djelfa, P.O. Box 3117, Djelfa 17000, Algeria; soulilahcene@univ-djelfa.dz

<sup>4</sup> Laboratoire Physico-Chimique des Matériaux et Environnement (LPCME), Faculty of Exact Sciences and Computer Science, University of Djelfa, P.O. Box 3117, Djelfa 17000, Algeria

<sup>5</sup> Unité Matériaux et Transformations (UMET), UMR8207, CNRS, INRAC, Centrale Lille, University Lille, 59000 Lille, France

\* Correspondence: y.derouiche@univ-djelfa.dz (Y.D.); ulrich.maschke@univ-lille.fr (U.M.); Tel.: +213-696-1-86-145 (Y.D.); +33-36-22-85-40-44 (U.M.)

**Abstract:** Galactomannan/organomodified montmorillonite (G<sub>1</sub>M/OM-MMT) nanocomposites and G<sub>2</sub>M/OM-MMT nanocomposites were biosynthesized using galactomannan (GM) and organomodified montmorillonite (OM-MMT) with cetyltrimethylammonium bromide (CTAB, 10<sup>-2</sup> M) designed for antioxidant activities. Furthermore, galactomannan (GM) was isolated from fruit rind of *Punica granatum* grown in the Djelfa region, in Algeria, and the nanoclay used in this work was an Algerian montmorillonite. Two different types of nanocomposites were synthesized using different amounts of GM and OM-MMT (*w/w*) [GM<sub>1</sub>/OM-MMT (0.5:1) and GM<sub>2</sub>/OM-MMT (0.5:2)] via a solution interaction method. FTIR analysis confirmed the intercalation of GM in the interlayer of OM-MMT. Moreover, X-ray diffraction (XRD) showed that the interlayer space of OM-MMT was increased from 124.6 nm to 209.9 nm, and regarding the intercalation of GM in the OM-MMT interlayers, scanning electron microscopy (SEM) and energy-dispersive X-ray (DEX) confirmed the intercalated structure of the nanocomposites, while thermogravimetric analysis (TGA) and differential scanning calorimetry (DSC) improved the thermal stability of the synthesized bionanocomposites. The antioxidant activities of the GM<sub>1</sub>/OM-MMT nanocomposites and GM<sub>2</sub>/OM-MMT nanocomposites were evaluated with a spectrophotometer and DPPH (1,1-diphenyl-2-picrylhydrazine) radical scavenging assay. GM<sub>1</sub>/OM-MMT nanocomposites and GM<sub>2</sub>/OM-MMT nanocomposites gave good antioxidant activity. Indeed, GM<sub>1</sub>/OM-MMT had an IC<sub>50</sub> of 0.19 mg/mL and GM<sub>2</sub>/OM-MMT an IC<sub>50</sub> of 0.28 mg/mL.

**Keywords:** nanocomposites; polysaccharide; *Punica granatum*; montmorillonite; biopolymer



check for updates

Academic Editor: Chih-Ching Huang

Received: 19 December 2024

Revised: 6 February 2025

Accepted: 8 February 2025

Published: 11 February 2025

**Citation:** Saihi, R.; Souli, L.; Chabira, S.F.; Derouiche, Y.; Maschke, U.

Synthesis and Characterization of Eco-Friendly Nanocomposites Using Galactomannan and Organomodified Montmorillonite. *Physchem* **2025**, *5*, 7. <https://doi.org/10.3390/physchem5010007>

**Copyright:** © 2025 by the authors.

Licensee MDPI, Basel, Switzerland.

This article is an open access article distributed under the terms and conditions of the Creative Commons Attribution (CC BY) license (<https://creativecommons.org/licenses/by/4.0/>).

## 1. Introduction

Bionanocomposites are synthesized from a biopolymer as matrix and an inorganic material as nanoclay; they have wide applications in different fields due to their biocompatibility and biodegradability [1]. Indeed, bionanocomposites are natural products based on agro-polymers extracted from biomass such as starch, cellulose and biodegradable polymers such as polylactic acid (PLA), polycaprolactone (PCL), poly(butylene succinate) (PBS) and polyhydroxybutyrate (PHB) [1]. The reinforcement most used in the synthesis of

bionanocomposites is montmorillonite since it has a nanometric structure and it has the power to modify the physico-chemical and mechanical characteristics of matrices based on polymers and biopolymers [2–4].

The range of applications and uses of bionanocomposites is vast. They are used in medicine [5] in pharmaceutical products, as they have antioxidant and antibacterial activity [6], but they are also used in hemodialysis, drug delivery, medical implants, scaffolding [7], biomedical devices, cosmetics [8] and non-steroidal anti-inflammatory drugs [9]. Galactomannan is a biodegradable and biocompatible biopolymer [10] obtained from legumes [11] such as *Astragalus gombiformis* Pomel (Fabaceae) [12], *Cassia fistula* [13], *Leucaena leucocephala* (Lam.) [14], *Ceratonia siliqua* seeds [15], *Cyamopsis tetragonoloba* [16,17] and fenugreek (*Trigonella foenum-graecum*) [18]. In addition, galactomannan is a heteropolysaccharide consisting of mannose and galactose units [19], and it has excellent antioxidant, immunomodulatory, antitumoral and antimetastatic activities [20,21], used in various biomedical applications [22,23]. It is applied in food, in pharmaceutical, in biomedical and in cosmetic industries due to its biocompatibility, water solubility and non-ionic properties [24–26], and it also has ionic stability and heat [27].

In this study, our objective is to synthesize a bionanocomposites designed for pharmaceutical applications using galactomannan extract from *P. granatum* as a polymer matrix and organomodified montmorillonite as a nanoclay. These bionanocomposites are natural, non-toxic and eco-friendly products.

## 2. Materials and Methods

### 2.1. Materials

Galactomannan (GM) was obtained by extraction from fruit rind of *punica granatum*, sodium chloride (Sigma-Aldrich company, Darmstadt, Germany), petroleum ether (Honeywell international Inc., Charlotte, NC, USA), cetyltrimethylammonium bromide (CTAB) (Honeywell international Inc., Charlotte, NC, USA), DPPH (Sigma-Aldrich company, Darmstadt, Germany), citric acid (Diagonostics Biochem Canada Inc., London, ON, Canada) and ethanol (Sigma-Aldrich company, Darmstadt, Germany) which were purchased and used as received, and all chemical reagents were of analytical reagent (AR) grade. Montmorillonite was obtained from the Bental National Company of Nonferrous Mining Products, Maghnia Unit, Algeria.

### 2.2. Isolation and Purification of Biopolymer

GM was extracted from fruit rind of *Punica granatum* from the Djelfa region located in central Algeria, following the protocol of Rao, Ghosh and Krishna with slight modifications [28]. A total of 40 g of *P. granatum* powder was macerated in 300 mL of petroleum ether at room temperature for 72 h; then, the extract was subsequently filtered and the solid part was dried and suspended in 1000 mL of cold water with stirring for the night. Then, it was filtered and the extract was concentrated to a reduced volume of 450 mL [28] and purified by dialysis using a 12–14 kD membrane for 24 h, followed by the precipitation of GM with ethanol dropwise for 3 h. This solution was maintained at 4 °C overnight to obtain a viscous yellow gel in water. This gel was separated by centrifugation at 6000 rpm for 10 min. The final product was separated using a freeze dryer.

### 2.3. Synthesis of Galactomannan/Organomodified Montmorillonite Nanocomposites

The montmorillonite used in this study is a 2:1 phyllosilicate composed of an octahedral metal–oxygen sheet sandwiched between two tetrahedral [SiO<sub>4</sub>] sheets, forming a sandwich structure with a thickness of 0.9 nm [29] and a cation exchange capacity (CEC) of 90 meq/g [30].

The organomodified montmorillonite (OM-MMT) was carried out as described by Loïc Lepluart [31]. A total of 10 g of MMT-Na<sup>+</sup> was dispersed in 100 mL of a 10<sup>-2</sup> M CTAB solution (3.64 g of CTAB). The mixture was heated to 80 °C with stirring for 3 h. Afterward, the OM-MMT was filtered, washed five times with double-distilled water, dried at 80 °C for 6 h, crushed and stored.

GM<sub>1</sub>/OM-MMT nanocomposites and GM<sub>2</sub>/OM-MMT nanocomposites were synthesized according to the method reported by Ponomarev [32]. For the synthesis of GM<sub>1</sub>/OM-MMT (0.5:1) and GM<sub>2</sub>/OM-MMT (0.5:2), two GM solutions (A and B) were prepared using 0.5 g of GM which was dissolved in 50 mL of deionized water and stirred for 30 min until its total dissolution. On the other hand, two solutions (A' and B') of organomodified montmorillonite were prepared using 1 g and 2 g of organomodified montmorillonite, respectively, and each amount of OM-MMT was mixed with 50 mL of deionized water and stirred for 4 h. These two solutions of galactomannan and OM-MMT were mixed (A mixed with A') and (B mixed with B') and left stirring for 24 h at room temperature. The obtained products were filtered and washed with a large amount of distilled water and ethanol until the filtrate was neutral. The final product was dried in an oven at 40 °C for 48 h and stored in a desiccator.

#### 2.4. In Vitro Antioxidant Assay

The antioxidant activity of GM<sub>1</sub>/OM-MMT nanocomposites and GM<sub>2</sub>/OM-MMT nanocomposites was determined using DPPH as a source of free radicals following the protocol described by Brand-Williams et al. [33]. Varying weights (0.03–1.0) mg of the GM<sub>1</sub>/OM-MMT nanocomposites and GM<sub>2</sub>/OM-MMT nanocomposites were mixed with 1 mL of water and dispersed by ultrasound for 30 min. A methanolic solution containing 0.2 mM of DPPH was prepared. A total of 1 mL of methanolic DPPH solution was added to each tube and left to stand for 30 min in the dark; then, the absorbance was measured at 517 nm. The following equation was used to calculate the percentage of inhibition of DPPH radicals [33]:

$$\% \text{ inhibition} = \frac{A_C - A_S}{A_C} \times 100 \quad (1)$$

where  $A_c$  is the absorbance of the control;  $A_s$  is the absorbance of the samples, after 30 min and measured at 517 nm.

#### 2.5. Characterization Methods

Fourier-transform infrared (FT-IR) spectra of the synthesized nanocomposites were obtained using IRTracer-100 with MIRacle 10 single reflection ATR accessory (Shimadzu Corporation, Kyoto, Japan). X-ray diffraction (XRD) measurement was carried out using an X-ray diffractometer (Empyrean PANalytical, Malvern Panalytical, Twente, The Netherlands) at 25 °C. Cu anode material: K-Alpha1 (1.54060 Å), K-lpha2 (1.54443 Å) and K-Beta (1.39225 Å), at 40 mA, and 45 kV were recorded in the region of 2θ from 3.0131 to 89.9831. Scanning electron microscopy (Quattro SEM, Thermo Fisher Scientific, Waltham, MA, USA) and energy-dispersive X-ray (DEX) analysis were performed using EDAX APEX software and with an accelerating voltage of 5 kV.

TGA, DSC (SETARAM LabsysEvo-gas, Lyon, France) analysis was performed under nitrogen gas (40 mL/min) in the temperature range of 28.22–800 °C, with a heating rate of 10 °C/min. Antioxidant study was conducted with an SP-UV 500DB/VDB Series UV-Vis spectrophotometer (Spectrum Instruments GmbH, Berlin, Germany).

### 3. Results and Discussion

#### 3.1. FT-IR Analysis

The FT-IR analyses of OM-MMT, GM<sub>1</sub>/OM-MMT nanocomposites and GM<sub>2</sub>/OM-MMT nanocomposites are shown in Figure 1. Broadbands in the region from 3623 cm<sup>-1</sup> are attributed to the stretching vibrations of the OH function of montmorillonite and galactomannan. There are bands at 2914 cm<sup>-1</sup> and 2859 cm<sup>-1</sup> corresponding to the C-H stretching vibrations (CH and CH<sub>2</sub>) of GM<sub>1</sub>/OM-MMT nanocomposites and GM<sub>2</sub>/OM-MMT nanocomposites [34]. The bands at 2357 cm<sup>-1</sup> and 1639.8 cm<sup>-1</sup> indicate absorbed water in the synthesized nanocomposites [35]. The bands at 1006 and at 917 cm<sup>-1</sup> are attributed to the stretching vibration of Si-O of the MMT and C-O of galactomannan. Another band is found at 848 cm<sup>-1</sup> for Al-OH, 785 cm<sup>-1</sup> due to (Al, Mg)-OH vibrations, and 523 and 436 cm<sup>-1</sup> for Si-O.

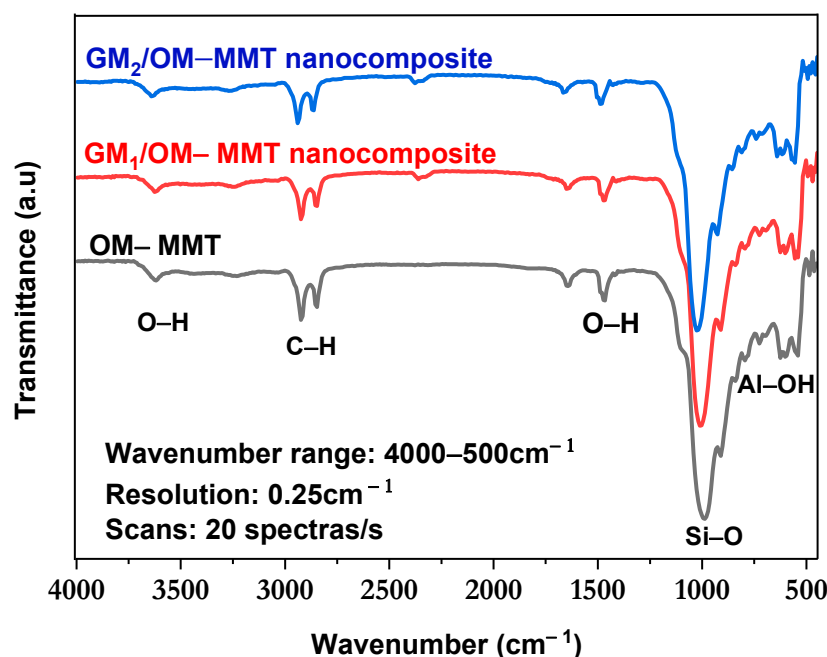


**Figure 1.** FT-IR spectrum of OM-MMT, GM<sub>1</sub>/OM-MMT nanocomposites and GM<sub>2</sub>/OM-MMT nanocomposites.

#### 3.2. X-Ray Diffraction (XRD)

Figure 2a illustrates the DRX of MMT-Na<sup>+</sup> and organomodified montmorillonite (OM-MMT). Figure 2b represents the XRD of GM<sub>1</sub>/OM-MMT and GM<sub>2</sub>/OM-MMT nanocomposites. In Figure 2a, the peak at 2θ = 7.267° (d<sub>001</sub> = 12.459 Å) corresponds to MMT-Na<sup>+</sup>. Other intense peaks are observed at 2θ = 19.85°, 27.30°, 31.77°, 45.45°, 56.44°, 66.75°, 75.24° and 84.04°. OM-MMT shows a peak at 2θ = 4.20° (d<sub>001</sub> = 209.9 nm), indicating the intercalation of CTAB into the MMT-Na<sup>+</sup> interlayer and the interlayer space was increased from 124.6 nm to 209.9 nm. Figure 2b illustrates the DRX of GM<sub>1</sub>/OM-MMT and GM<sub>2</sub>/OM-MMT nanocomposites with different concentrations of GM. In the diffractogram, there are montmorillonite peaks located at 2θ: 19°, 26° and 64°. Other peaks with different intensities observed on the diffractogram are attributed to the OM-MMT and indicate that the latter is partially or totally intercalated by the GM [36].

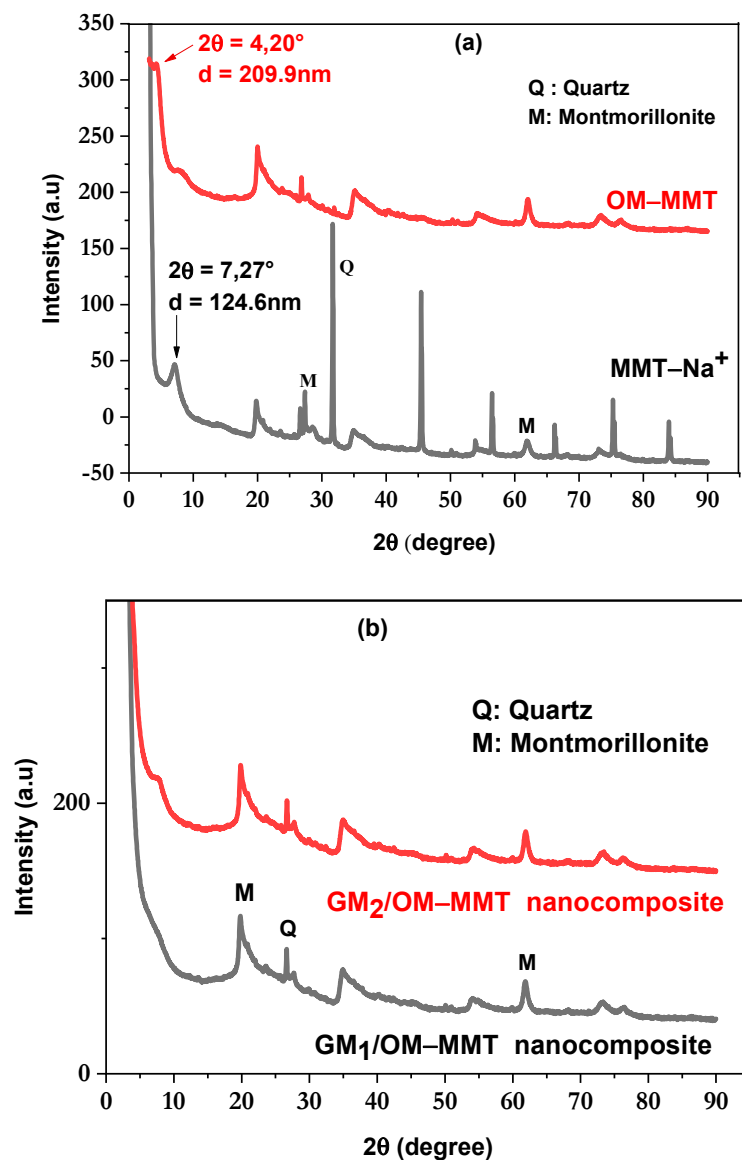
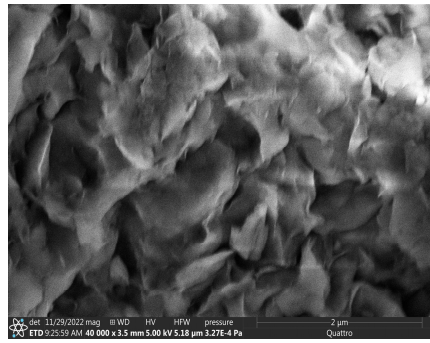


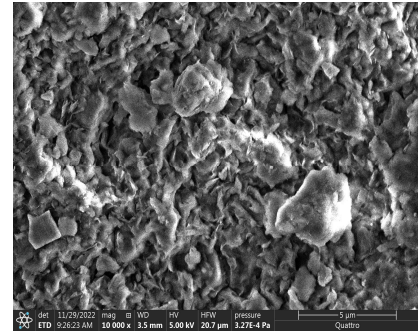
**Figure 2.** XRD patterns of (a) MMT-Na<sup>+</sup> and OM-MMT, (b) GM<sub>1</sub>/OM-MMT nanocomposites and GM<sub>2</sub>/OM-MMT nanocomposites.

### 3.3. Morphological Investigation of Bionanocomposites and EDX Analysis

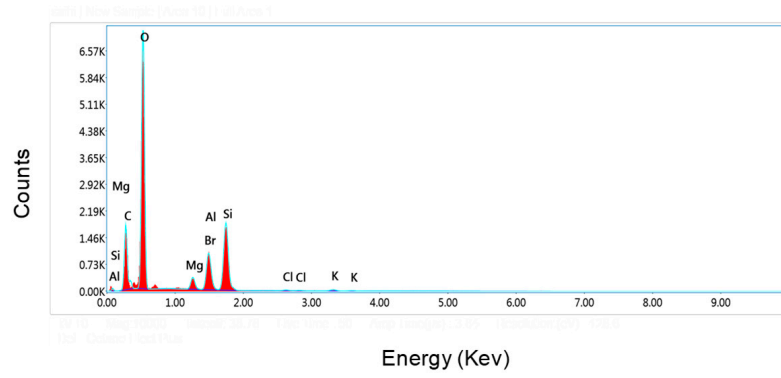
Figure 3 shows the morphology and EDX of OM-MMT, the synthesized GM<sub>1</sub>/OM-MMT and GM<sub>2</sub>/OM-MMT nanocomposites investigated by SEM and EDX. The SEM images of OM-MMT are shown in Figure 3a,b, those of GM<sub>1</sub>/OM-MMT nanocomposites are shown in Figure 3d,e and those of GM<sub>2</sub>/OM-MMT nanocomposites are presented in Figure 3g,h. All the images clearly reveal that the surface morphology of the samples features both rough and smooth areas, organized in sheet-like structures. These areas display large cavities and a compacted surface, resulting from the dispersion of galactomannan within the intercalated montmorillonite.



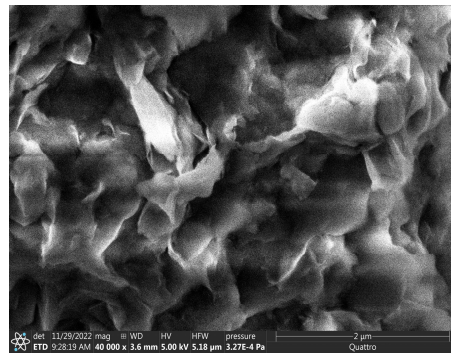
(a)



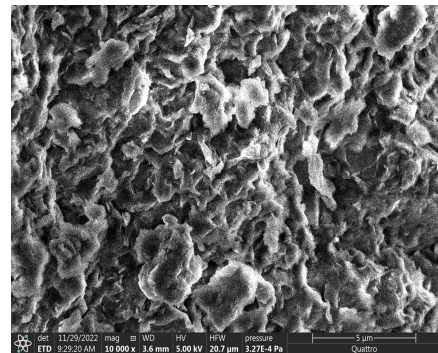
(b)



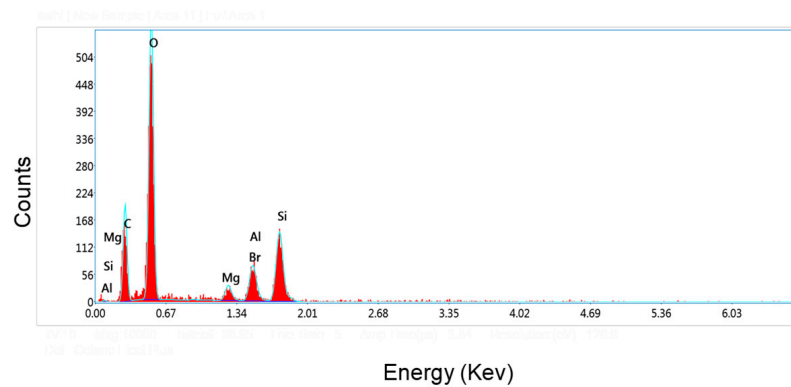
(c)



(d)



(e)



(f)

Figure 3. Cont.

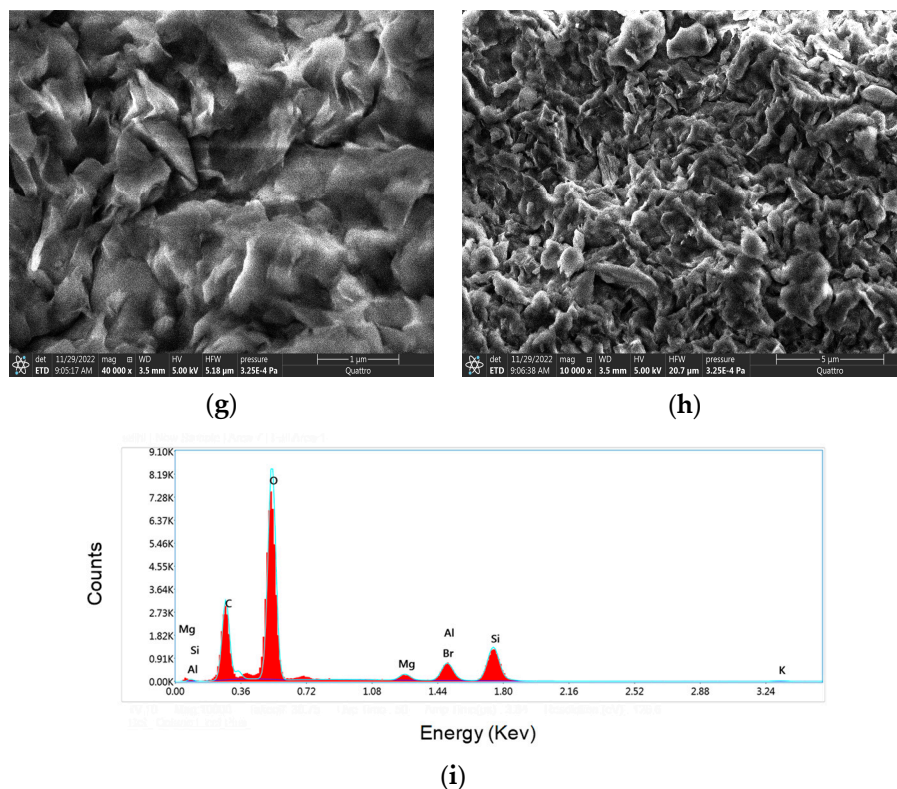


**Figure 3.** SEM images of (a) (2  $\mu\text{m}$ , 40,000 $\times$ ), (b) (5  $\mu\text{m}$ , 10,000 $\times$ ) and (c) EDX of OM-MMT. (d) (2  $\mu\text{m}$ , 40,000 $\times$ ), (e) (5  $\mu\text{m}$ , 10,000 $\times$ ) and (f) EDX of GM1/OM-MMT nanocomposites, (g) (1  $\mu\text{m}$ , 40,000 $\times$ ), (h) (5  $\mu\text{m}$ , 10,000 $\times$ ) and (i) EDX of GM2/OM-MMT nanocomposites.

Figure 3c,f,i show the EDX spectra for the OM-MMT, GM<sub>1</sub>/OM-MMT nanocomposites and GM<sub>2</sub>/OM-MMT nanocomposites, respectively. The peaks detected between 0 and 1 keV of the GM<sub>1</sub>/OM-MMT nanocomposites (Figure 3f) and GM<sub>2</sub>/OM-MMT nanocomposites (Figure 3i) represent the binding energies of OM-MMT (Al, Si, Mg and GM (C and O)).

In addition, the peaks found between 1 and 2 keV of OM-MMT (Figure 3c), of GM<sub>1</sub>/OM-MMT (Figure 3f), of GM<sub>2</sub>/OM-MMT (Figure 3i) correspond to the binding energies of MMT–Mg, Al, Si and Br. The quantitative calculation obtained by EDX is presented in the Table 1a for OM-MMT, in Table 1b for GM<sub>1</sub>/OM-MMT nanocomposites and in Table 1c for GM<sub>2</sub>/OM-MMT nanocomposites, and these results confirm the presence of elemental compounds of the OM-MM and GM. The percentage weights obtained for GM1/OM–MMT nanocomposites and for GM2/OM–MMT nanocomposites are similar.

### 3.4. Thermal Stability

The TGA analyses of OM-MMT, GM<sub>1</sub>/OM-MMT nanocomposites and GM<sub>2</sub>/OM-MMT nanocomposites are shown in Figure 4a, 4b and 4c, respectively. A total of 14.51 mg, 10.16 mg and 15.24 mg of each sample of OM-MMT, GM<sub>1</sub>/OM-MMT nanocomposites and GM<sub>2</sub>/OM-MMT nanocomposites, respectively, were analyzed. For the OM-MMT, a thermal decomposition in three steps is seen. In addition, an initial weight loss of 0.4 mg (2.5%) was observed between 28.3 and 159.0  $^{\circ}\text{C}$ , which can be attributed to the loss of adsorbed water. A total of 2.6 mg (17.9%) was lost between 159.0 and 350.7  $^{\circ}\text{C}$ , which may be due to CTAB degradation. Finally, in the temperature range of 349.5–795.9  $^{\circ}\text{C}$ , a mass of 1.98 mg (13.6%) was lost and it was attributed to the mineral composition of montmorillonite.

**Table 1.** Percentage of chemical elements obtained by EDX analysis of (a) OM-MMT, (b) GM<sub>1</sub>/OM-MMT nanocomposites and (c) GM<sub>2</sub>/OM-MMT nanocomposites.

(a) OM-MMT								
Element	CK	OK	MgK	AlK	SiK	ClK	KK	Br L
Weight(%)	19.9	51.8	2.9	4.6	15.7	0.4	0.1	4.5
Atomic(%)	28.8	55.8	1.5	2.9	9.6	0.2	0.4	0.9
(b) GM <sub>1</sub> /OM-MMT nanocomposite								
Element	CK	OK	MgK	AlK	SiK	Br L		
Weight(%)	29.2	48.4	2.8	3.2	12.8	4.1		
Atomic(%)	39.4	49.0	1.4	1.9	7.4	0.8		
(c) GM <sub>2</sub> /OM-MMT nanocomposite								
Element	CK	OK	MgK	AlK	SiK	KK	Br L	
Weight(%)	25.9	56.2	1.5	3.5	10.3	0.6	1.9	
Atomic(%)	34.5	55.9	0.9	2.1	5.8	0.2	0.4	

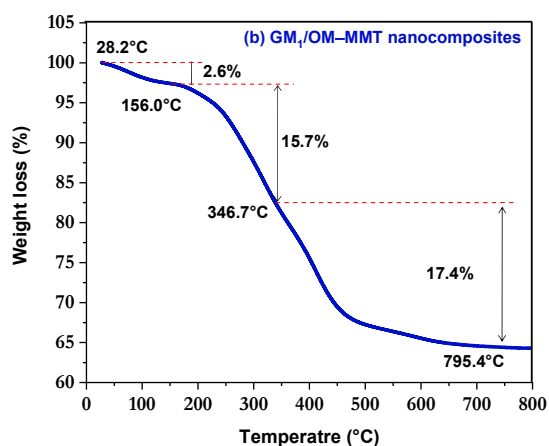
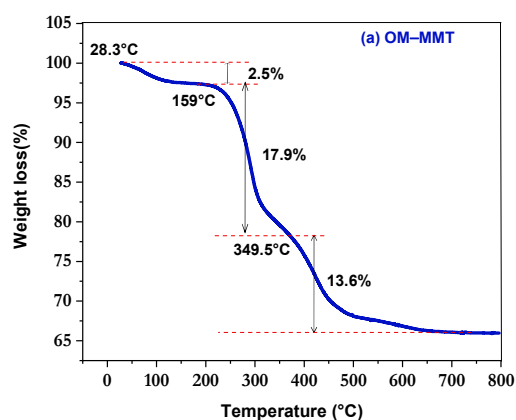


**Figure 4.** Cont.

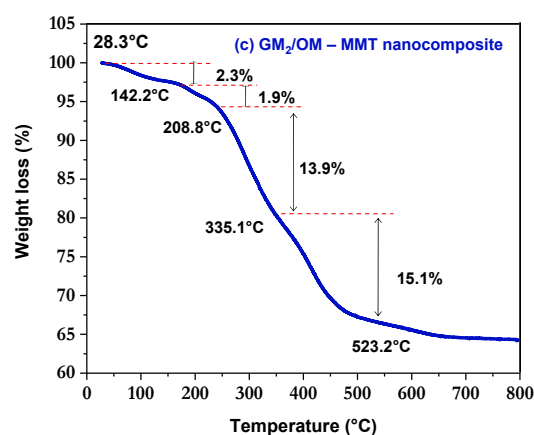


**Figure 4.** Thermogravimetric analysis (TGA) of (a) OM-MMT, (b) GM<sub>1</sub>/OM-MMT nanocomposites and (c) GM<sub>2</sub>/OM-MMT nanocomposites.

The nanocomposites show thermal decomposition in different steps, the first one being close to 150.0 °C, which is attributed to the loss of adsorbed water in the GM<sub>x</sub>/OM-MMT nanocomposites. A weight loss of 0.269 mg (2.6%) was observed for GM<sub>1</sub>/OM-MMT and a weight loss of 0.3 mg (2.3%) was obtained for GM<sub>2</sub>/OM-MMT.

The second weight loss was found between 155.1 °C and 346.7 °C of 1.6 mg (15.7%) for GM<sub>1</sub>/OM-MMT and is attributed to galactomannan degradation. In addition, a weight loss of 0.3 mg (1.9%) was observed for GM<sub>2</sub>/OM-MMT between 142.2 and 208.8 °C due to CTAB decomposition. The thirist mass loss is observed between 345.2 and 795.5 °C of 1.8 mg (17.4%) for GM<sub>1</sub>/OM-MMT, and is attributed to the decomposition of the mineral composition of montmorillonite. For GM<sub>2</sub>/OM-MMT, a weight loss is observed between 208.2 °C and 335.1 °C of 2.1 mg (13.9%), which is attributed to the galactomannan decomposition, and a fourth weight loss was observed between 334.9 °C and 523.3 °C of 2.3 mg (15.1%) for GM<sub>2</sub>/OM-MMT, which is attributed to the decomposition of the mineral composition of montmorillonite.

### 3.5. DSC Analysis

The DSC analyses of OM-MMT, GM<sub>1</sub>/OM-MMT nanocomposites and GM<sub>2</sub>/OM-MMT nanocomposites are shown in Figure 5a, 5b and 5c, respectively. A total of 14.5 mg, 10.7 mg and 15.2 mg of each sample of OM-MMT, GM<sub>1</sub>/OM-MMT nanocomposites and GM<sub>2</sub>/OM-MMT nanocomposites, respectively, were analyzed and heated from 28.6 to 800 °C at a scan rate of 10 °C/min.

DSC curves of organomodified montmorillonite (OM-MMT) have endothermic peaks at 39.56, 291.0 and at 434.5 °C, with the first of the glass transition (T<sub>g</sub>) with enthalpy of 566.1 J/g (29.7–124.5 °C). The second peak is the first melting temperature (T<sub>m1</sub> = 291.0 °C) with melting enthalpy, ΔH<sub>m1</sub> = 44.8 J/g, and the third peak is the second melting temperature (T<sub>m2</sub> = 334.5 °C) with second melting enthalpy (ΔH<sub>m2</sub> = 84.1 J/g).

DSC curves of GM<sub>1</sub>/OM-MMT nanocomposites have endothermic peaks at 41.2, at 261.2, at 322.5 and at 427.4 °C, the first of the glass transition T<sub>g</sub> = 28.8 °C and an enthalpy of 377.9 J/g (Onset: 28.8 °C, Offset: 139.3 °C). The second, third and fourth peaks represent the melting temperatures (261.2 °C, 322.5 °C and 427.4 °C), and melting enthalpies of 9.9, 0.6 and 46.3 J/g. On the other hand, the DSC curves of GM<sub>2</sub>/OM-MMT nanocomposites also have four endothermic peaks at 40.2, 277.3, 330.8 and at 444.2 °C, and the first of the glass transition with an enthalpy of 323.7 J/g. The second, third and fourth peaks represent the melting temperatures of 277.4, 330.8 and 444.2 °C, with melting enthalpies of 323.7, 12.7, 1.6 and 42.7 J/g, respectively.

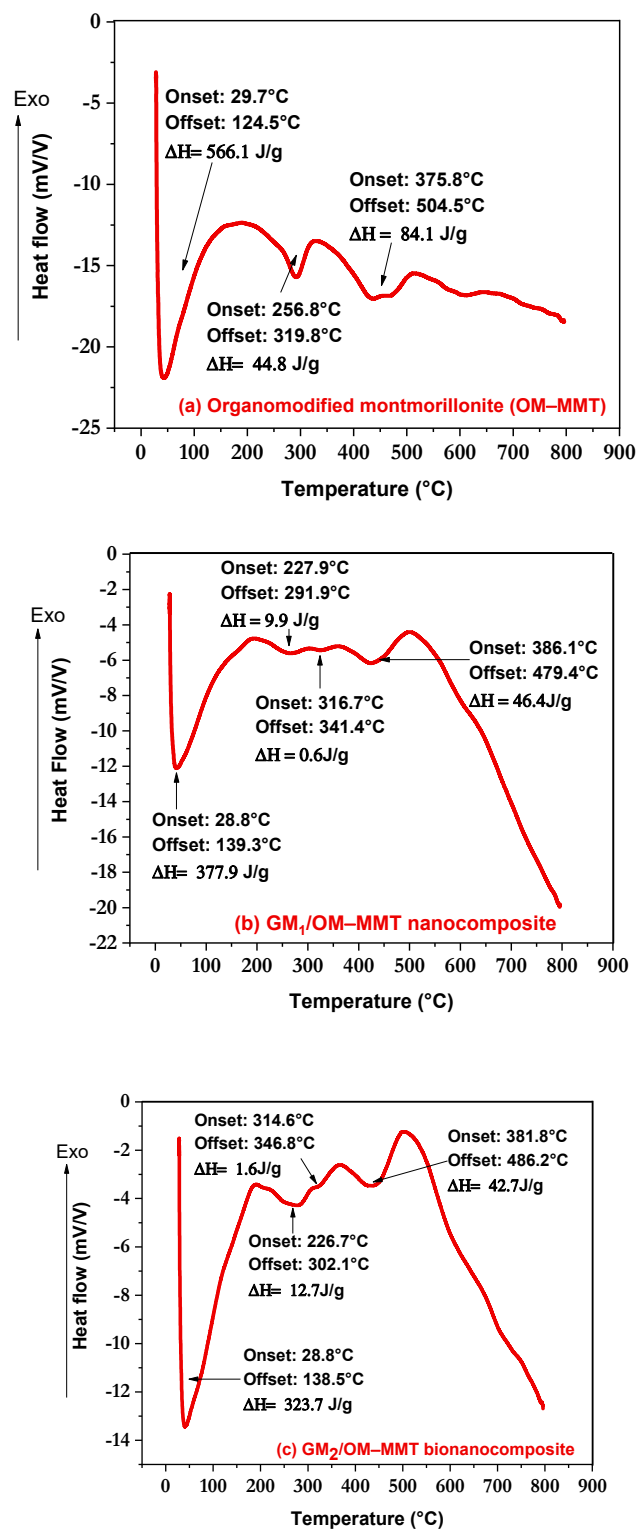


**Figure 5.** DSC thermograms of (a) OM-MMT, (b) GM<sub>1</sub>/OM-MMT nanocomposites and (c) GM<sub>2</sub>/OM-MMT nanocomposites.

The compositions of the GM<sub>1</sub>/OM-MMT and GM<sub>2</sub>/OM-MMT nanocomposites influenced the thermal behavior of the nanocomposites. The TGA and DSC thermograms of the nanocomposites are different from those of OM-MMT.

### 3.6. In Vitro Antioxidant Discussion

The antioxidant activities of GM<sub>1</sub>/OM-MMT and GM<sub>2</sub>/OM-MMT nanocomposites were tested through the diphenyl-2-picrylhydrazyl (DPPH) assay. The DPPH free radicals were confined in the interlayers of the nanocomposites and then trapped, and could subsequently be neutralized. In this study, the in vitro antioxidant potential of GM<sub>1</sub>/OM-MMT nanocomposites and GM<sub>2</sub>/OM-MMT nanocomposites was evaluated against DPPH (Figure 6). It was observed that the percentage (Figure 7) of DPPH scavenging activity of GM<sub>1</sub>/OM-MMT nanocomposites was 62.3%, higher than that of GM<sub>2</sub>/OM-MMT nanocomposites, which was of 61.8% at different concentrations (0.033 to 1.0 mg/mL). Comparatively, GM<sub>1</sub>/OM-MMT nanocomposites exhibit higher free radical scavenging activity than GM<sub>2</sub>/OM-MMT nanocomposites, and this is perhaps reflected in the concentration of the biopolymers used in the synthesis of the nanocomposites. The obtained IC<sub>50</sub> values for GM<sub>1</sub>/OM-MMT nanocomposites and GM<sub>2</sub>/OM-MMT nanocomposites were 0.19 mg/mL and 0.28 mg/mL, respectively.

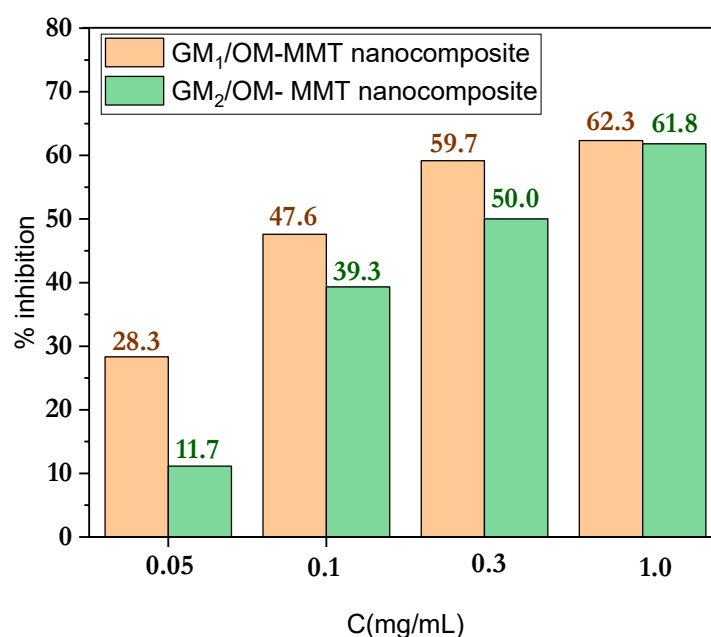


**Figure 6.** Comparison of DPPH radical scavenging activity between GM<sub>1</sub>/OM-MMT nanocomposites and GM<sub>2</sub>/OM-MMT nanocomposites.

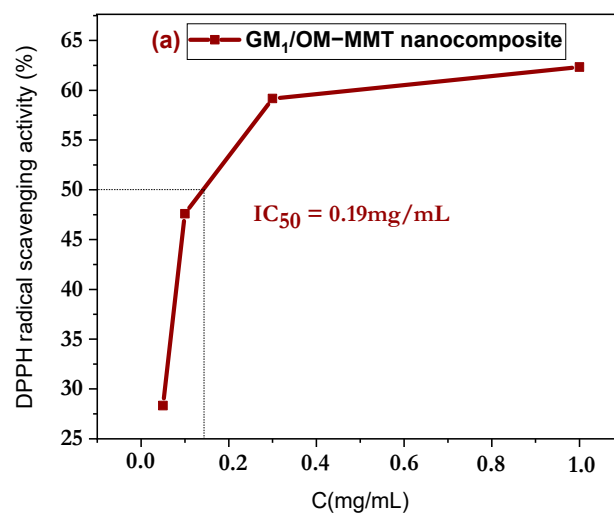


**Figure 7.** Cont.

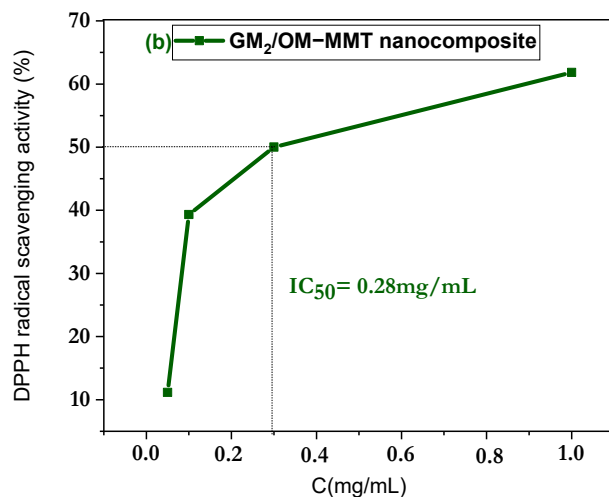


**Figure 7.** DPPH radical scavenging activity of (a) GM<sub>1</sub>/OM-MMT nanocomposites and (b) GM<sub>2</sub>/OM-MMT nanocomposites.

### 3.7. DPPH Radical Scavenging Mechanism

GM<sub>1</sub>/OM-MMT and GM<sub>2</sub>/OM-MMT nanocomposites are rich in hydroxyl groups (-OH) due to the presence of galactomannan [37]. They can release hydrogen radicals followed by rapid transfer of liberated hydrogen protons and DPPH free radicals to scavenge free radicals (Figure 8). Compounds that have hydroxyl groups in them are good antioxidants. Furthermore, ascorbic acid is a very good antioxidant; it is able to release two hydrogen radicals per molecule from its hydroxyl groups [38,39]. Phenolic compounds also have antioxidant properties by releasing hydrogen radicals from hydroxyl groups and can subsequently scavenge free radicals [40].

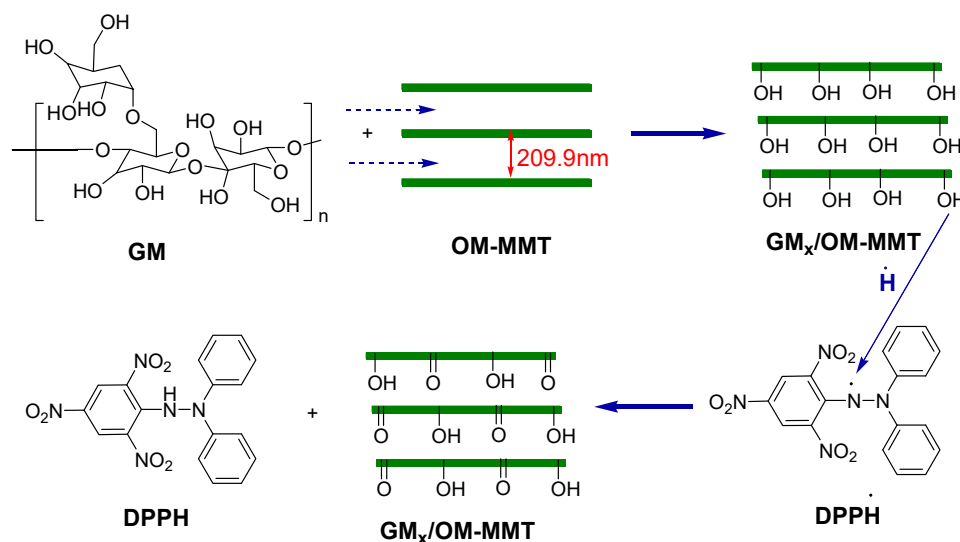


**Figure 8.** Scheme of the scavenging of DPPH free radicals by GM<sub>1</sub>/OM-MMT and GM<sub>2</sub>/OM-MMT nanocomposites.

## 4. Conclusions

In this study, GM<sub>1</sub>/OM-MMT and GM<sub>2</sub>/OM-MMT nanocomposites were prepared using organomodified montmorillonite (OM-MMT) and galactomannan (GM) as natural and eco-friendly products. In addition, OM-MMT was obtained by chemically modifying crude montmorillonite with cetyltrimethylammonium bromide (CTAB). The gallery spacing of organomodified montmorillonite was increased from 124.6 to 209.9 nm, and this increase

allowed the biopolymer to intercalate into the galleries of OM-MM. Furthermore, GM was extracted from fruit rind of *punicagranatum* and was a water-soluble, biodegradable, biocompatible and non-toxic biopolymer. The synthesis of nanocomposites was carried out by solution intercalation using the deionized water as a solvent. The FT-IR analysis clearly confirms the intercalation of GM in the gallery of montmorillonite by the presence of C-H and C-O vibration bands of the GM at 2900–2800  $\text{cm}^{-1}$  and at 1006.5  $\text{cm}^{-1}$ , respectively. The disappearance or reduction in the montmorillonite peaks at 35°, 55° and 74° indicates the intercalation of the biopolymer into the interlayers of OM-MMT. Moreover, the SEM-EDX analyses are in agreement with the results of the XRD analysis. Analysis by TGA shows that the OM-MMT and synthesized nanocomposites are very thermally stable. During the heating of OM-MMT, GM<sub>1</sub>/OM-MMT and GM<sub>2</sub>/OM-MMT nanocomposites, which took place between room temperature and 800 °C, several mass losses were observed for OM-MMT and for nanocomposites with different percentages, confirming that the materials have different compositions. At 795.5 °C and 523.2 °C, respectively, GM<sub>1</sub>/OM-MMT nanocomposites and GM<sub>2</sub>/OM-MMT nanocomposites lost all chemical and mineral composition. The inhibition percentages of DPPH radicals by the GM<sub>1</sub>/OM-MMT and GM<sub>2</sub>/OM-MMT nanocomposites are of 62.3% and 61.8% and the graphically calculated IC<sub>50</sub> values are of 0.19 mg/mL and 0.28 mg/mL, respectively. The process of DPPH free radical inhibition is based on the confinement and inhibition of DPPH radicals within the nanocomposite galleries.

**Author Contributions:** Conceptualization, L.S., S.F.C. and R.S.; methodology, R.S.; L.S. and S.F.C.; validation, Y.D., U.M., L.S. and S.F.C.; formal analysis, R.S. and L.S.; investigation, S.F.C., L.S., Y.D. and U.M.; data curation, R.S. and L.S.; writing—original draft preparation, R.S. and L.S.; writing—review and editing, S.F.C., Y.D. and U.M.; visualization, L.S. and S.F.C.; supervision, L.S. and S.F.C. All authors have read and agreed to the published version of the manuscript.

**Funding:** This research received no external funding.

**Data Availability Statement:** Data are contained within the article.

**Acknowledgments:** The authors gratefully acknowledge the support of the Algerian Ministry of Higher Education and Scientific Research (MESRS), the General Directorate of Scientific Research and Technological Development (DGRSDT) of Algeria, the University of Djelfa/Algeria.

**Conflicts of Interest:** The authors declare no conflicts of interest.

## Nomenclature

GM	Galactomannan
OM-MMT	Organomodified montmorillonite
DPPHD	Phenyl-2-picrylhydrazyl
IC <sub>50</sub>	Half-maximal inhibitory concentration

## References

1. Rajendra, K.K.; Anshuman, S. Recent Developments in Bio-nanocomposites: A Review. *Res. J. Nanosci. Eng.* **2018**, *2*, 1–4.
2. Zhang, Y.P.; Wang, X.; Shen, Y.; Thakur, K.; Zhang, J.-G.; Hu, F.; Wei, Z.-J. Preparation and Characterization of Bio-Nanocomposites Film of Chitosan and Montmorillonite Incorporated with Ginger Essential Oil and Its Application in Chilled Beef Preservation. *Antibiotics* **2021**, *10*, 796. [[CrossRef](#)] [[PubMed](#)]
3. Proença, L.B.; Righetto, G.M.; da Cunha Camargo, I.L.B.; Branciforti, M.C. Poly(acid lactic)-montmorillonite clay bionanocomposites loaded with tea tree oil for application in antibacterial wound healing. *Hybrid Adv.* **2024**, *6*, 100201. [[CrossRef](#)]
4. Krzykowska, B.; Uram, Ł.; Frańcz, W.; Kovářová, M.; Sedlařík, V.; Hanusova, D.; Kisiel, M.; Paciorek-Sadowska, J.; Borowicz, M.; Zarzyka, I. Polymer Bionanocomposites Based on a P<sub>3</sub>BH/Polyurethane Matrix with Organomodified Montmorillonite-Mechanical and Thermal Properties, Biodegradability, and Cytotoxicity. *Polymers* **2024**, *16*, 2681. [[CrossRef](#)]

5. Botta, L.; La Mantia, F.P.; Mistretta, M.C.; Oliveri, A.; Arrigo, R.; Malucelli, G. Structure-property relationships in bionanocomposites for pipe extrusion applications. *Polymers* **2021**, *13*, 782. [[CrossRef](#)]
6. Lizundia, E.; Armentano, I.; Luzi, F.; Bertoglio, F.; Restivo, E.; Visai, L.; Torre, L.; Puglia, D. Synergic Effect of Nanolignin and Metal Oxide Nanoparticles into Poly(L-lactide) Bionanocomposites: Material Properties, Antioxidant Activity, and Antibacterial Performance. *ACS Appl. Bio Mater.* **2020**, *3*, 5263–5274. [[CrossRef](#)]
7. Zielińska, A.; Karczewski, J.; Eder, P.; Kolanowski, T.; Szalata, M.; Wielgus, K.; Szalata, M.; Kim, D.; Shin, S.R.; Słomski, R.; et al. Scaffolds for drug delivery and tissue engineering: The role of genetics. *J. Ophthalmol. Clin. Res.* **2023**, *359*, 207–223. [[CrossRef](#)]
8. Akbar, M.U.; Athar, M.M.; Bhatti, I.A.; Bhatti, H.N.; Khosa, M.K.; Zia, K.M. Chapter 17—Biomedical applications of bionanocomposites. In *Bionanocomposites, Green Synthesis and Applications Micro and Nano Technologies*; Elsevier: Amsterdam, The Netherlands, 2020; pp. 457–483. [[CrossRef](#)]
9. Joshi, G.; Yadav, K.S. Chapter 2—Applications of bioresins and biopolymers derived from natural resources as composites in drug delivery. In *Green Sustainable Process for Chemical and Environmental Engineering and Science*; Elsevier: Amsterdam, The Netherlands, 2023; pp. 21–34.
10. Reddy, K.; Mohan, G.K.; Satla, S.; Gaikwad, S. Natural polysaccharides: Versatile excipients for controlled drug delivery systems. *Asian J. Pharm. Sci.* **2011**, *6*, 275.
11. Ozen, I.; Bahtiyari, I.M.; Haji, A.; ul Islam, S.; Wang, X. Properties of galactomannans and their textile-related applications—A concise Review. *Int. J. Biol. Macromol.* **2023**, *227*, 1001–1014. [[CrossRef](#)]
12. Bouziane, G.; Henni, A.; Bouricha, M.; Boual, Z.; Belkhalifa, H.; Bachari, K.; Didi Ould El Hadj, M. A new galactomannan extracted from the seeds of *Astragalus gombiformis* Pomel (Fabaceae) and its utilization in the biosynthesis of silver nanoparticles. *Process Biochem.* **2024**, *136*, 48–59. [[CrossRef](#)]
13. Pandey, J.; Singh, B.D.; Khanam, H.; Tiwari, B.; Azaz, T.; Singh, R. Cassia fistula galactomannan stabilized copper nanocatalyst as an efficient, recyclable heterogeneous catalyst for the fast clickable [3+2] Huisgen cycloadditions in water. *Int. J. Biol. Macromol.* **2024**, *255*, 128098. [[CrossRef](#)] [[PubMed](#)]
14. Mittal, N.; Kaur, G. *Leucaena leucocephala* (Lam.) galactomannan nanoparticles: Optimization and characterization for ocular delivery in glaucoma treatment. *Int. J. Biol. Macromol.* **2019**, *139*, 1252–1262. [[CrossRef](#)] [[PubMed](#)]
15. Srivastava, M.; Kapoor, V.P. Seed galactomannans: Overview. *Chem. Biodivers.* **2005**, *2*, 295–317. [[CrossRef](#)]
16. Sharma, P.; Sharma, S.; Ramakrishna, G.; Srivastava, H.; Gaikwad, K. A comprehensive review on leguminous galactomannans: Structural analysis, functional properties, biosynthesis process and industrial applications. *Crit. Rev. Food Sci. Nutr.* **2021**, *62*, 443–465. [[CrossRef](#)]
17. Mirhosseini, H.; Amid, B.T. A review study on chemical composition and molecular structure of newly plant gum exudates and seed gums. *Food Res. Int.* **2012**, *46*, 387–398. [[CrossRef](#)]
18. Zhu, Y.; Xu, W.; Feng, C.; Zhu, L.; Ji, L.; Wang, K.; Jiang, J. Study on structure and properties of galactomannan and enzyme changes during fenugreek seeds germination. *Carbohydr. Polym.* **2024**, *327*, 121653. [[CrossRef](#)]
19. Wang, W.; McConaghy, A.M.; Tetley, L.; Uchegbu, I.F. Controls on polymer molecular weight may be used to control the size of palmitoyl glycol chitosan polymeric vesicles. *Langmuir* **2001**, *17*, 631–636. [[CrossRef](#)]
20. Joseph, M.M.; Aravind, S.; Varghese, S.; Mini, S.; Sreelekha, T. Evaluation of antioxidant, antitumor and immunomodulatory properties of polysaccharide isolated from fruit rind of *Punica granatum*. *Mol. Med. Rep.* **2012**, *5*, 489–496.
21. Varghese, S.; Joseph, M.M.; Aravind, S.; Unnikrishnan, B.; Sreelekha, T. The inhibitory effect of anti-tumor polysaccharide from *Punica granatum* on metastasis. *Int. J. Biol. Macromol.* **2017**, *103*, 1000–1010. [[CrossRef](#)]
22. Nalbantova, V.; Benbassat, N.; Delattre, C. Fenugreek Galactomannan and Its Versatile Applications. *Polysaccharides* **2024**, *5*, 478–492. [[CrossRef](#)]
23. Prajapati, V.D.; Jani, G.K.; Moradiya, N.G.; Randeria, N.P.; Nagar, B.J.; Naikwadi, N.N.; Variya, B.C. Galactomannan: A versatile biodegradable seed polysaccharide. *Int. J. Biol. Macromol.* **2013**, *60*, 83–92. [[CrossRef](#)] [[PubMed](#)]
24. Shahbuddin, M.; Shahbuddin, D.; Bullock, A.J.; Ibrahim, H.; Rimmer, S.; MacNeil, S. High molecular weight plant heteropolysaccharides stimulate fibroblasts but inhibit keratinocytes. *Carbohydr. Res.* **2013**, *375*, 90–99. [[CrossRef](#)] [[PubMed](#)]
25. Albuquerque, P.B.S.; Barros, W.; Santos, G.R.C.; Correia, M.T.S.; Mourão, P.A.S.; Teixeira, J.A.; Carneiro-Da-Cunha, M.G. Characterization and rheological study of the galactomannan extracted from seeds of *Cassia Grandis*. *Carbohydr. Polym.* **2014**, *104*, 127–134. [[CrossRef](#)] [[PubMed](#)]
26. Pinheiro, A.C.; Bourbon, A.I.; Rocha, C.; Ribeiro, C.; Maia, J.M.; Goncalves, M.P.; Vicente, A.A. Rheological characterization of carrageenan/galactomannan and xanthan/galactomannan gels: Comparison of galactomannans from non-traditional sources with conventional galactomannans. *Carbohydr. Polym.* **2011**, *83*, 392–399. [[CrossRef](#)]
27. Sittikijyothin, W.; Torres, D.; Gonçalves, M.P. Modelling the rheological behaviour of galactomannan aqueous solutions. *Carbohydr. Polym.* **2005**, *59*, 339–350. [[CrossRef](#)]
28. Rao, P.S.; Ghosh, T.P.; Krishna, S. Extraction and purification of tamarind seed polysaccharide. *J. Sci. Ind. Res.* **1946**, *4*, 705.

29. Sajjadi, M.; Baran, N.Y.; Baran, T.; Nasrollahzadeh, M.; Tahsili, M.R.; Shokouhimehr, M. Palladium nanoparticles stabilized on a novel Schiff base modified Unye bentonite: Highly stable, reusable and efficient nanocatalyst for treating wastewater contaminants and inactivating pathogenic microbes. *Sep. Purif. Technol.* **2020**, *237*, 116383. [[CrossRef](#)]
30. Khelifi, A.; Boubberka, Z.; Bentaleb, K.; Hamani, H.; Derrich, Z. Removal of 2, 4-DCP from wastewater by CTAB/bentonite using one-step and two-step methods: A comparative study. *Chem. Eng. J.* **2009**, *164*, 345–354. [[CrossRef](#)]
31. Lepluart, L. Nanocomposites, Epoxyde, Amine, Montmorillonite: Role of Interactions on The Formation, Morphology at Different Levels of Scale and Mechanical Properties of The Networks. Ph.D. Thesis, National Institute of Applied Sciences, Lyon, France, 2002.
32. Ponomarev, N.; Repo, E.; Srivastava, V.; Sillanpää, M. Green thermal-assisted synthesis and characterization of novel cellulose-Mg(OH)<sub>2</sub> nanocomposite in PEG/NaOH solvent. *Carbohydr. Polym.* **2017**, *176*, 327–335. [[CrossRef](#)]
33. Brand-Williams, W.; Cuvelier, M.E.; Berset, C. Use of a free radical method to evaluate antioxidant activity. *LWT-Food. Sci. Technol.* **1995**, *28*, 25–30.
34. Fronza, P.; Batista, M.J.P.A.; Franca, A.S.; Oliveira, L.S. Bionanocomposite Based on Cassava Waste Starch, Locust Bean Galactomannan, and Cassava Waste Cellulose Nanofibers. *Foods* **2024**, *13*, 202. [[CrossRef](#)] [[PubMed](#)]
35. Shamel, K.; Bin Ahmad, M.; Zargar, M.; Wan Yunus, W.M.Z.; Ibrahim, N.A.; Shabanzadeh, P.; Moghaddam, M.G. Synthesis and characterization of silver/montmorillonite/chitosan bionanocomposites by chemical reduction method and their antibacterial activity. *Int. J. Nanomed.* **2011**, *6*, 271–284. [[CrossRef](#)] [[PubMed](#)]
36. Liu, X.; Wu, Q. PP/clay nanocomposites prepared by grafting melt Intercalation. *Polymers* **2001**, *42*, 10013–10019. [[CrossRef](#)]
37. Mark, Q.G.; Xinzhong, H.; Changlu, W.; Lianzhong, A. Polysaccharides: Structure and solubility. *Solubility Polysacch.* **2017**, *2*, 8–21. [[CrossRef](#)]
38. Gegotek, A.; Skrzydlewska, E. Antioxidative and Anti-Inflammatory Activity of Ascorbic Acid. *Antioxidants* **2022**, *11*, 1993. [[CrossRef](#)]
39. Angeli, L.; Morozova, K.; Scampicchio, M. A kinetic-based stopped-flow DPPH• method. *Sci. Rep.* **2023**, *13*, 7621. [[CrossRef](#)]
40. Becerril-Sánchez, A.L.; Quintero-Salazar, B.; Dublán-García, O.; Escalona-Buendía, H.B. Phenolic Compounds in Honey and Their Relationship with Antioxidant Activity, Botanical Origin, and Color. *Antioxidants* **2021**, *10*, 1700. [[CrossRef](#)]

**Disclaimer/Publisher's Note:** The statements, opinions and data contained in all publications are solely those of the individual author(s) and contributor(s) and not of MDPI and/or the editor(s). MDPI and/or the editor(s) disclaim responsibility for any injury to people or property resulting from any ideas, methods, instructions or products referred to in the content.